Liquid Crystals

ISSN: 0267-8292 (Print) 1366-5855 (Online) Journal homepage: https://www.tandfonline.com/loi/tlct20

Ray optics simulations of polarised microscopy textures in chiral nematic droplets

Urban Mur, Simon Čopar, Gregor Posnjak, Igor Muševič, Miha Ravnik & Slobodan Žumer

To cite this article: Urban Mur, Simon Čopar, Gregor Posnjak, Igor Muševič, Miha Ravnik & Slobodan Žumer (2017) Ray optics simulations of polarised microscopy textures in chiral nematic droplets, Liquid Crystals, 44:4, 679-687, DOI: 10.1080/02678292.2016.1230788

To link to this article: https://doi.org/10.1080/02678292.2016.1230788

LIQUID CRYSTALS, 2017
VOL. 44, NO. 4, 679–687
https://doi.org/10.1080/02678292.2016.1230788

Taylor & Francis
Taylor & Francis Group

Ray optics simulations of polarised microscopy textures in chiral nematic droplets

Urban Mur[a], Simon Čopar[a], Gregor Posnjak[b], Igor Muševič[a,b], Miha Ravnik[a,b] and Slobodan Žumer[a,b]

[a]Faculty of Mathematics and Physics, University of Ljubljana, Ljubljana, Slovenia; [b]Condensed Matter Physics Department, Jožef Stefan Institute, Ljubljana, Slovenia

ABSTRACT

We present a simple method for simulating optical polarised micrographs of director fields in optically birefringent structures. Jones matrix method is applied for simulating polarised micrographs with focusing optics that can sufficiently account for different focusing distances and numerical apertures (NAs) in the polarised microscopy, which are the typical experimental variables. Accuracy of the method is assessed by comparing experimental and numerical micrographs of various structures in cholesteric liquid crystal droplets. The effects of varied focusing distance and scale are tested. The performance of the developed method is further demonstrated by varying viewing direction, position of focusing plane and the size of the observed structure, which prove to be elementary and easily changed parameters of this approach.

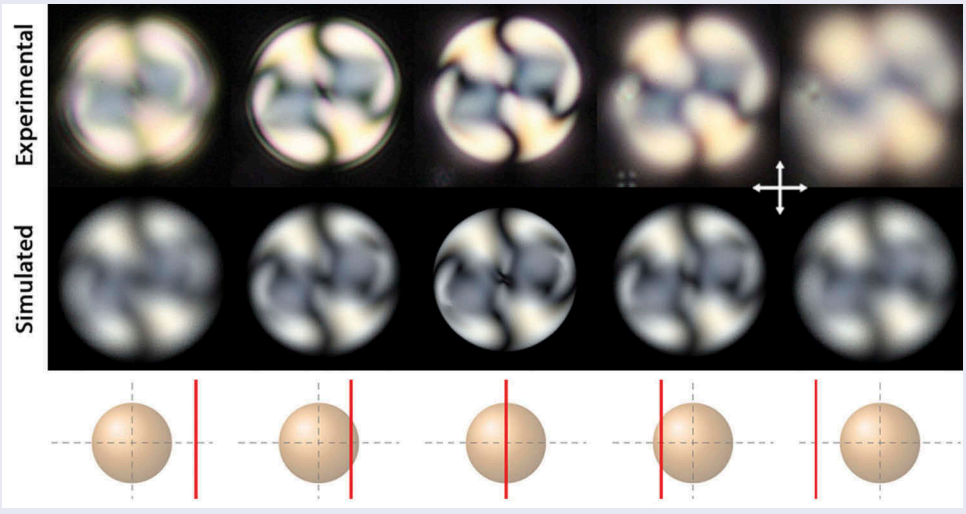

ARTICLE HISTORY
Received 23 June 2016
Accepted 27 August 2016

KEYWORDS
Polarised microscopy; cholesteric droplets; chiral nematic; texture simulations; ray optics

1. Introduction

Liquid crystals (LCs) are optically anisotropic fluids [1], which combine the fluidity of ordinary fluids with optical birefringence. The birefringence of LCs is due to the long-range orientational order of rod-like LC molecules. The polarisibility of LC molecules is different for an electric field oscillating along or transverse to the long molecular axis, and the speed of light in LCs strongly depends on the direction and polarisation of light. The resulting difference in the extraordinary (n_e) and ordinary (n_o) refractive indices depends on the degree of collective orientational order and molecular anisotropy and can be as high as $n_e - n_o \sim 0.4$. It is the basis of practically all optical applications of LCs, including LC displays [2], microlasers [3–5], phase modulators [6], wave guides [7] and antennas [8].

The orientational ordering of the molecules is well responsive to external stimuli over a broad range of length scales (10 nm to 10 μm) and time scales (ps to ms) which is the result of inherent softness of the collective orientational phenomena. A major experimental and theoretical effort in LC research is to develop novel birefringent structures by controlling the orientational order via external fields, surfaces, chirality, by adding colloidal particles of various complexity or forming

CONTACT Slobodan Žumer slobodan.zumer@fmf.uni-lj.si Faculty of Mathematics and Physics, University of Ljubljana, Ljubljana, Slovenia

droplets [9,10]. Selected recent results include topological colloids [11], three-dimensional (3D) orthorombic colloidal nanocrystals [12], blue phase gels [13], nematic colloidal knots [14], colloidal opals as memory materials [15], colloidal-cholesteric composites [16] and emerging LC microphotonics [17]. The fundamental challenge in designing such materials and more complex photonic systems is to understand and experimentally determine the spatial profile of birefringence and liquid crystalline order.

Modern approaches for determining profiles of nematic order are all based on optical microscopy and include stimulated Raman scattering microscopy [18], fluorescence polarised microscopy [19] and multiphoton microscopy [20], with the standard approaches being bright field transmission microscopy, which more clearly discerns the singular defect lines, and polarised optical microscopy (POM), which is sensitive to the director field orientation and reveals defects through the characteristic dark brushes in the micrograph [21]. Polarised microscopy is based on illuminating the sample with polarised light with the sample placed between crossed polarisers. Due to birefringence, a phase shift between the two orthogonal components of initial polarisation is obtained. Phase shifts are transformed to intensity profile with the analyser which reveals, neglecting effects of light refraction and scattering, the profile of the nematic order. Theoretically, within such approximation, the polarised microscopy can be described via Jones 2 × 2 matrix formalism, using simple ray optics [22]. The approach uses matrices to represent the mixing and phase delay of orthogonal polarisation states imposed by a thin slab of birefringent material. Intensity of transmitted light is obtained by evaluating the product of these matrices across the sample thickness, applying it to the incoming polarisation, and projecting onto the analyser direction. For simplicity of calculation, parallel rays are commonly used [23], usually aligned along the principal axes of the input data lattice, which disregards focusing properties of the imaging optics. This reduces the similarity between the Jones matrix calculated images and the experimentally gathered images and may lead to ambiguously recognised structures in more complicated samples.

The motivation for this development of adapted ray optics method is the notable recent development in the techniques for characterisation of nematic orientational fields [24,25] and advanced simulations of complex defects and textures in nematic systems [26]. Especially, chiral and achiral nematic LC droplets are recently attracting a lot of attention, because of their distinct geometry [27–29].

In this article, we present a simple method for modelling light transmission through samples of optically anisotropic materials by generalising the Jones matrix approach, which accounts also for non-parallel light rays, i.e. light focusing due to usually quite large NA of the optical microscope. Complex birefringent structures in cholesteric LC droplets are used as test examples for studying the effects of birefringence on the polarised microscopy image. We assess the results of the numerical method against experimental POM observations, where fluorescent confocal polarised microscopy (FCPM) data is used as input for the nematic director. Compared to the simpler Jones matrix method, which uses parallel rays, adding a lens between the droplet and the screen accurately reproduces focusing behaviour, which turns out to be an essential feature of microscope optics. Having full control over the orientation and optical parameters in simulation, the sample can be numerically imaged at different orientations, focus distances and droplet sizes, allowing identification of many experimental micrographs without repeating the more elaborate confocal imaging process. The method is also fast, which is a notable advantage over other more involved numerical simulations which take into account the wave nature of light.

2. Description of the method

In a polarised microscope, the birefringent sample is put between two crossed polarisers, i.e. the polariser on the side of incidence and the analyser on the opposite side. The accumulation of phase of the electromagnetic wave, which is different for two eigen polarisations of incident light, results in a Schlieren texture [30].

The core of our method is the propagation of a single ray through the sample, calculated with the Jones calculus, where the ray can have an arbitrary direction, as required by the geometry of the simulated optics and the aperture. Such approach allows us to choose arbitrary viewing direction and simulate focusing. The nematic director data along the ray are obtained with the interpolation from the values on the points of a grid used in the numerical or experimental determination of the nematic field, as shown in Figure 1(a) for a simple two-dimensional case. Optical anisotropy is computed in the plane perpendicular to the direction of the ray.

Employing Jones calculus, the relative intensity of the transmitted light on the screen for each ray can be determined as

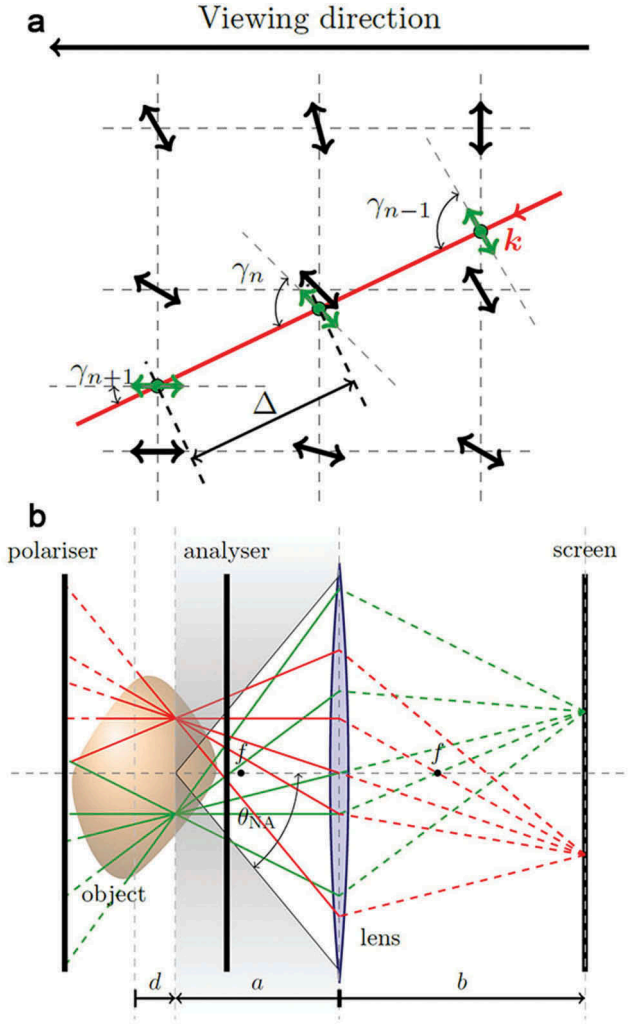

Figure 1. Scheme of the generalised method and the geometry of the considered set-up. (a) Representation of director field interpolation along the ray. The director nearest to the sampling point is used, and the angle γ between the ray and the director is calculated. Black arrows in the picture represent the nematic director field and red line demonstrates the propagation of ray in the direction of $\vec{k}$. In the actual simulation, the director and the ray are in three spatial dimensions. (b) Paths of light rays that contribute to each pixel in the image, the lens and the polarisers used in the method. Each ray is propagated directly from the lens through the imaging point in focusing plane which lies at the chosen distance d from the centre of the sample. Solid lines are the actual simulated ray paths and dashed lines show the path to the screen where the intensity is accumulated. *a, b* and *f* represent the denoted distances used in geometry optics equations. θ_{NA} shows the maximum angle allowed by the lens aperture.

$$I = \sum_{\lambda} I_0(\lambda) |\boldsymbol{e}_A \boldsymbol{T} \boldsymbol{e}_P|^2, \tag{1}$$

where unit vectors $\boldsymbol{e}_A$ and $\boldsymbol{e}_P$ describe the directions of analyser and polariser axes, expressed in the frame perpendicular to each light ray. The angles of incidence are in practice close enough to perpendicular so that polarisers function as intended. The Jones matrix T describes the total modulation of light on its way through the sample. $I_0(\lambda)$ is the intensity of illumination at each chosen wavelength λ, to allow summation over the spectrum of the light used to illuminate the sample. The image is normalised to use the entire intensity range of the output image format.

The Jones matrix T is calculated numerically by dividing the nematic sample into discrete intervals Δ, thin enough that the director field can be assumed homogeneous inside [21]. With such construction, the problem is divided into a succession of propagations through the slab with homogeneous director field and the cumulative matrix is computed by successive multiplication of Jones matrices for a slab [23]. At every step, the phase shift between the ordinary and extraordinary ray is calculated. The phase shift δ is given by

$$\delta = 2\pi \frac{\Delta}{\lambda} (n_e(\gamma) - n_o) \tag{2}$$

where λ is the vacuum wave length of incident light, Δ is thickness of a thin slab and $n_e(\gamma)$ is the extraordinary index of refraction, which depends on the angle γ between the ray direction and the local optical axis,

$$n_e(\gamma) = \frac{n_o n_e}{\sqrt{n_o^2 \sin^2 \gamma + n_e^2 \cos^2 \gamma}}. \tag{3}$$

The local optical axis in LCs corresponds to the local nematic director and can be calculated from the Q-tensor, as well explained in [31]. In the experiment, it can be reconstructed directly from experimental data using FCPM [24].

We model the optical imaging system as a single ideal lens with a circular aperture, as shown in Figure 1 (b). Instead of one ray per pixel, as used in the method with parallel rays, many rays are needed for each point on the simulated image. In our case, 1000 rays were sent from every pixel, which proves to be enough for a sufficiently sharp image while keeping the computational cost relatively low. We assume perfect focusing, so that each point on a focusing plane corresponds to a single point on the image plane. We use the reciprocity theorem: instead of propagating the rays from the light source, we generate a pencil of rays going through each point on the focusing plane, knowing they all contribute to the same pixel on the image plane. Thus we ensure enough rays for each pixel of the image without tracing stray rays (Figure 1(b)). The angles of the rays are limited by the lens aperture and by the collimation of the light source, whichever is more restrictive, which

is measured by the NA. Ray directions within the allowed range are generated by randomly selecting the intersection with the lens, following an appropriate angular probability distribution. Each ray is then propagated directly from the intersection through the chosen point on the focusing plane. As only the ray path through the object contributes to the transmittance calculation, the distance between the lens and the screen is irrelevant and is assumed to be such that the lens equation is satisfied. Contributions of single rays to the image are summed by intensity, as we are simulating an incoherent illumination source.

The main parameter that governs appearance of the micrograph is NA which determines the maximum angle at which rays pass through the sample. It is a characteristic parameter of the objective used for microscopy, and the simulation is calibrated to match the experiment. Note that the rays refract at the interface from air to the cell containing the sample (in our case the droplet and index-matched host liquid around it), so the effective NA in the medium is smaller by the factor of index of refraction. Additionally, if the illumination is collimated, it can result in effectively smaller NA. Larger NA means narrower depth of field and thus stronger effect of defocusing, but in transmission microscopy, the entire sample contributes to the micrograph, regardless of the position of the focusing plane. Even with the focus at the centre of the sample, transmittance differs for different ray angles, which may visibly affect most of the appearance of the micrograph for larger NAs. In our simulations, $NA = 0.1$ was used as the best match with the experiments.

The method allows control of the following parameters: viewing direction, numerical aperture of the lens *NA* and the distance of focusing plane to the centre of the sample, marked as d in the Figure 1(b). Parameters that can also be controlled in the parallel ray Jones method are the spectrum of the illuminating light, ordinary and extraordinary refraction index, the orientations of polariser and analyser and, if present, other optical elements, such as phase retardation plates. For a non-monochromatic light, the intensity profile is summed over different wavelengths weighted by spectral intensity ratios of these wavelengths, approximating the real illumination spectrum (e.g. black body spectrum approximation at a given temperature or a measured light spectrum).

3. The experiment

As a model system with sufficient complexity to test this method, we choose chiral nematic droplets, dispersed in a carrier fluid [32]. The experimental samples are prepared by dispersing a small amount of a LC in a mixture of glycerol and 4 % L-alpha-phosphatidylcholine (lecithin), which ensures perpendicular anchoring of LC molecules on the surface of the droplets. We use a 1:1 weight ratio mixture of two LCs with very low birefringence: 4′-butyl-4-heptyl-bicyclohexyl-4-carbonitrile (CCN-47) and 4,4′-dipentyl-bicyclohexyl-4-carbonitrile (CCN-55). This mixture has a nematic phase at room temperature and the nematic to isotropic phase transition is above 60°C. This mixture of CCN LCs is chosen because of its low birefringence and close index matching to glycerol ($n_{ord} = 1.47$ and $n_{ext} = 1.50$; $n_{glycerol} = 1.47$), which facilitates reconstruction of the director field from FCPM data with few artefacts and diminishes lensing effects which are not accounted for in our ray optics method [24]. To achieve the desirable chiral pitch of ($5 - 10$ μm), the LC mixture is doped with chiral dopant S-811 (1–2 %). The cells are prepared by sandwiching the LC/glycerol mixture between a 1-mm-thick glass plate and a 150 μm cover glass, separated by 30 μm spacers and sealed with a two-component epoxy glue. The transmission micrographs are taken with a Canon 550D digital camera used on a Nikon Eclipse E-600 microscope with Nikon LU Plan 100 × N = 0.9 air objective with crossed polariser and analyser. In addition to polarised microscopy, the same droplets were imaged with a fluorescent confocal polarised microscopy. For the FCPM experiments, a Leica TCS SP5 X confocal system based on an Leica DMI6000B inverted motorised microscope was used and the LC was fluorescently labelled, as described in detail in [24].

When a cell containing LC dispersion is prepared, POM indicates that numerous droplet structures can occur. Earlier studies have shown that many different director profiles at random orientations are found, containing point topological defects, embedded in skyrmion and toron-like structures [24]. These 3D director structures are reconstructed from FCPM images taken at different polarisations using recently developed algorithm described in [24]. Importantly, this experimentally extracted 3D director field inside the droplet is then used as an input for the calculations of polarised microscopy images, presented in this work. To demonstrate the validity of our numerical method, we choose two different director structures reconstructed from FCPM experiments, one with three collinear point defects along the diameter of the droplet and one with two point defects and a defect ring. These structures are very common in chiral nematic droplets with perpendicular surface anchoring and the ratio of the droplet diameter $2R$ to the half-pitch $p/2$ around $2d/p \sim 3$.

To verify the direction-dependent simulated polarised micrographs, we use several different droplets found in our sample with different orientations. The droplets are selected according to their typical visual appearance between crossed polarisers [24].

4. Results

We compare experimental polarised micrographs with their simulated counterparts, where the director used in simulated micrographs was derived from the FCPM images of the same droplets. The droplet diameters are $\approx$ 20μm, the distance between droplet and the lens is set in calculations to 1.5 mm and refractive indices are set to match the experimental values.

In Figure 2, the comparison between white light experimental and calculated polarised micrographs is shown for a nematic droplet with 3 point defects upon changing the focus and for two different viewing directions. Indeed, the calculations reproduce the effects that are created during the light propagation through the droplet, even when the focusing plane is not centred in the middle of the droplet. When droplet is out of focus, the micrographs are blurred, which is well seen in Figures 2 and 5.

To show that the droplet shown in Figure 2(a–j) has the same structure as the droplet in Figure 2(l–v), just rotated differently, we have simulated micrographs in both Figure 2(f–j) and Figure 2(q–u) using the confocal data from the first droplet (Figure 2(a–e)). The same parameters of numerical calculation were used in both cases except the direction of the incident light. Good qualitative agreement with POM experiments is achieved for the rotated droplet, which not only confirms the similarity of both imaged droplets, but also verifies that the director field reconstruction from FCPM is accurate enough to produce the same optical transmission image.

When comparing results with micrographs created by use of simpler Jones matrix method [22], which uses parallel rays, no significant differences have been observed between micrographs (Figure 3), when focusing plane is in the middle of the droplet and NA $\leq$ 0.1. However, the simple Jones method cannot reproduce micrographs for displacements of focusing plane inside the droplet (compare Figure 3 with Figure 2(a–j)), which can help us recognise structures of director field in droplets that are out of focus.

Figure 4 shows numerically generated images of the same droplet as in Figure 2, but for a wider range of

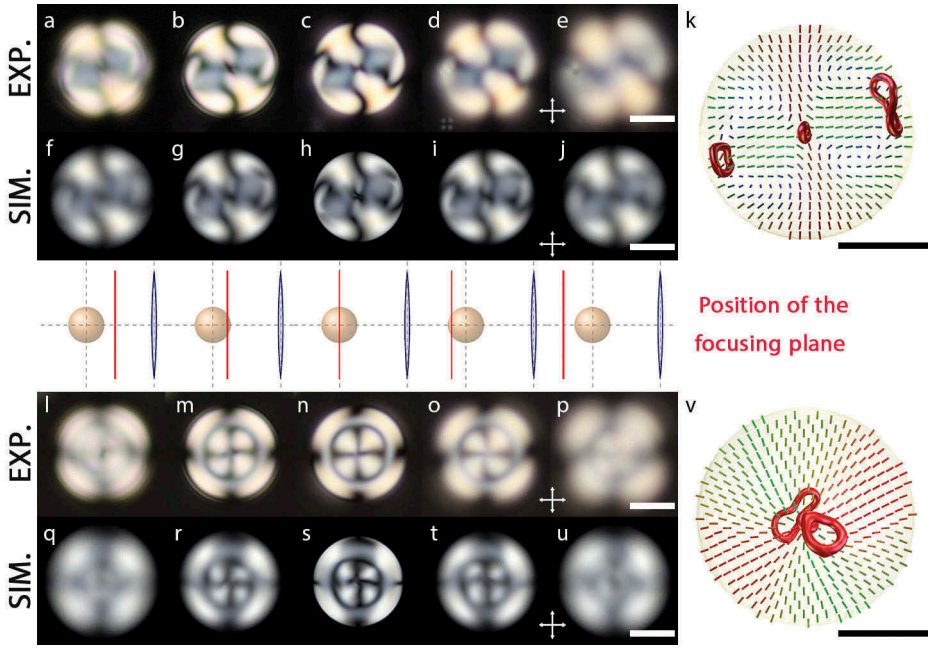

Figure 2. Comparison between experimental POM (a–e, l–p) and corresponding simulated (f–j, q–u) micrographs of a structure with 3 point defects in nematic droplet for different positions of focusing plane and two viewing directions. Focusing plane was moved in steps of 8 μm (i.e. 0.8*R*, where *R* is the droplet radius). Panel (k) shows visualisation of the FCPM experimental reconstruction of 3 defects and director field in the same viewing direction as the simulated and experimental micrographs (a–e, f–j). Note that the appearance of the point defects as small defect loops is a result of the limitations of FCPM experiment and reconstruction algorithm. Experimental (l–p) and numerical micrographs (q–u) correspond to the same structure, viewed along the symmetry axis of the structure, which is perpendicular to the viewing direction in (a–k). The FCPM data used for POM simulation, shown in (v) is the same as in (k), only rotated. Crossed double arrows indicate the directions of polariser and analyser, scale bar corresponds to 10 μm. Cylinders in (k,v) represent the director, coloured to better distinguish different directions.

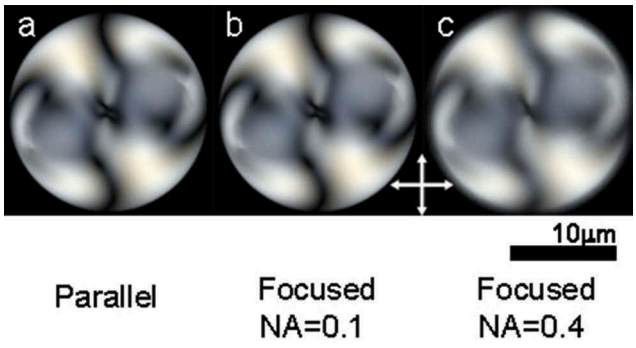

Figure 3. Comparison between numerical micrographs for parallel (a) and focused rays (b, c) The same droplet and orientation as in Figure 2(a–j) was used. Only for *NA* = 0.1, no significant difference between the parallel and focused rays is observed if the droplet's focusing plane goes through the centre of the droplet.

viewing directions, revealing how the same droplet can look very different at different angles. One can clearly see that it is difficult to recognise or even conjecture on the 3D structure, if the symmetry axis is not aligned with the viewing direction. This is quite common in an emulsion, where the orientations of the symmetry axis (if any) of droplets are random.

Figure 5 shows white light micrographs (a-j) for a droplet with 2 points and a large loop defect (Fig. 5k) and was used to test the method on a different structure than in Figure 2. The region around the disclination loop is discernible as a darker band in both experiment and simulation, signifying that additional optical effects, such as scattering, lensing and absorption in the defect core – also neglected in our simulations of polarised micrographs – have small effect on the appearance of the micrograph. The monochromatic micrograph (l) that closely resembles white light ones (c, h) confirms that for low birefringent materials textures brushes depend on the predominant director orientation along the ray accompanied by Mauguin kind polarization rotation.

When the LC is dispersed into the glycerol with simple mixing, droplets of many sizes are created [32]. Generally, the size and the pitch-to-size ratio both affect the structure formation. However, qualitatively similar structures with the same arrangement of topological defects can be seen in droplets of different sizes, so FCPM data acquired for one such droplet may be used to simulate micrographs for scaled versions of the droplet. Thus, the same structure can be identified in droplets of different sizes, even for droplet sizes, which are not suitable for FCPM imaging.

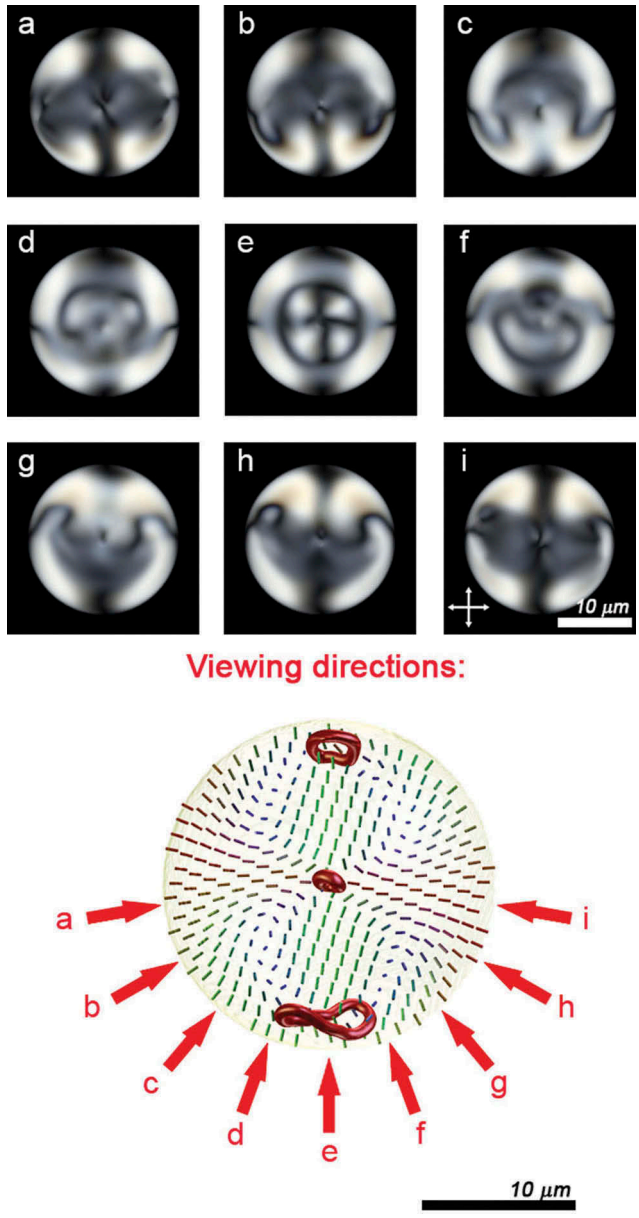

Figure 4. Simulated micrographs of the droplet from Figure 2 for different viewing directions, changed in steps of 20° in relation to the symmetry axis of the defect structure. Viewing directions of each micrograph are marked with red arrows, as viewed from the above.

Keeping the pitch-to-size ratio fixed, the physical size of the system (i.e. in the presented case, the droplet radius) only enters the polarised micrograph calculations through the ratio between the wavelength λ and the step along the ray Δ when computing the phase shift (Equation (2)). Figure 6 shows the polarised micrographs of the droplet shown in Figure 2 only now scaled to different physical sizes. Medium sized droplets additionally show typical optical interference fringes of different colours in white light (Figure 6(a,c)) and monocromatic (Figure 6(b)) with λ = 575 nm light,

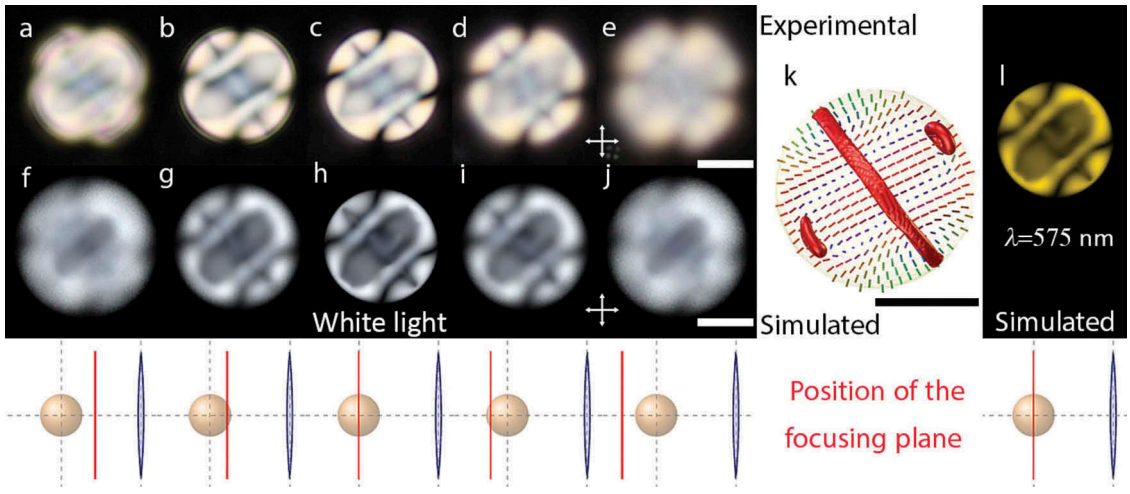

Figure 5. Comparison of experimental (a–e) and simulated (f–j) micrographs for 2 point + loop defect structure in a cholesteric droplet. The focusing plane is moved in 8 μm steps. The far left pictures represent the plane which is closest to the lens. (k) The director structure in the droplet as reconstructed from FCPM experiment, viewed from the same direction as in the polarised micrographs. (l) Monochromatic micrograph at $\lambda = 575$ nm focused on the midplane (as panels (c) and (h)). Scale bar represents 10 μm and crossed double arrows indicate the directions of polariser and analyser.

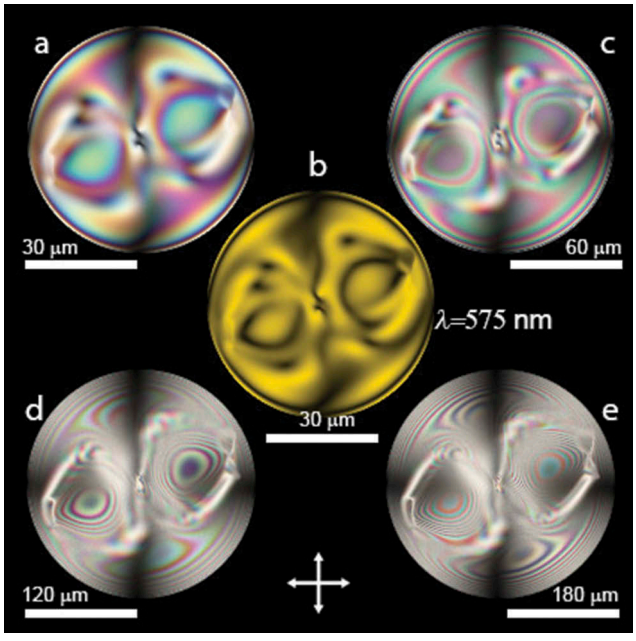

Figure 6. Numerical polarised micrographs of different sized droplets ((a,c–e) in white and (b) in $\lambda = 575$ nm light). Value of diameter in comparison to wavelengths of illuminating light was changed, but keeping the pitch-to-size ratio constant. Droplet with 3 point defects and the same viewing direction as in Figure 2(a–j) was used. Diameters in panels (a–e) are set to $2R \approx \{60, 60, 120, 240, 360\}$ μm, respectively; other parameters are kept fixed.

while for monocromatic light interference fringes not observed in smaller droplets (Fig. 2) are even more clear. Larger droplets (Figure 6(d,e)) show a different, more uniform images, where numerous fringes are practically no more resolved. The results show that the presented method can be used at good qualitative level also for extrapolating polarised micrographs to different physical scales, of course under condition that the structure itself does not change significantly under the change in scales.

5. Conclusion

We demonstrated the use of generalised Jones polarisation formalism, adapted to real microscopy technique. The numerical method accounts for non-parallel light rays, variable light focusing, different light spectra, and imaging from arbitrary direction with respect to a fixed frame. We used different cholesteric LC droplets as test examples of complex spatially varying birefringence and non-trivial geometry. Notably, the method can be used to compare different droplets sizes or orientations and could be used as a strong tool to determine unknown structures with minimal number of 3D confocal experiments. Very good qualitative agreement between numerical and experimental micrographs is demonstrated, even though the method is based on ray optics and neglects refraction, scattering, lensing and absorption within the sample. For the materials with larger birefringence the method could be further upgraded by including refraction within the sample, as caused by spatial variation of the index of refraction due to birefringence. The method could also take into account optical aberrations produced

by real lenses, absorption and scattering inside the sample, and coherent illumination.

To account for diffraction effects, more advanced methods for wave optics are needed, such as finite-difference time-domain (FDTD)-based simulations [33]. Such methods are computationally intensive, require careful interpretation of the results and are not suitable as a quick visualisation step. This was the reason for developing a method capable of presenting experimentally reconstructed or simulation-generated nematic fields in complex geometries.

Disclosure statement

No potential conflict of interest was reported by the authors.

Funding

The Authors acknowledge funding from Air Force Office of Scientific Research [FA9550-15-1-0418] and Javna Agencija za Raziskovalno Dejavnost RS [J1-6723, J1-7300, P1-0099].

References

[1] de Gennes PG, Prost J. The physics of liquid crystals. New York (NY): Oxford University Press; 1993.
[2] Schadt M. Liquid crystal materials and liquid crystal displays. Annu Rev Mater Sci. 1997;27(1):305–379. DOI:10.1146/annurev.matsci.27.1.305
[3] Hur S, Lee B, Gim M, et al. Liquid-crystalline blue phase laser with widely tunable wavelength. Adv Mater. 2013;25(21):3002–3006. DOI:10.1002/adma.201204591
[4] Humar M, Muševič I. 3D microlasers from self-assembled cholesteric liquid-crystal microdroplets. Opt Express. 2010;18(26):26995–27003. DOI:10.1364/OE.18.026995
[5] Coles H, Morris S. Liquid-crystal lasers. Nature Photonics. 2010;4(10):676–685. DOI:10.1038/nphoton.2010.184
[6] Love G. Liquid-crystal phase modulator for unpolarized light. Appl Opt. 1993;32(13):2222–2223. DOI:10.1364/AO.32.002222
[7] Zografopoulos D, Asquini R, Kriezis E, et al. Guided-wave liquid-crystal photonics. Lab Chip. 2012;12(19):3598–3610. DOI:10.1039/c2lc40514h
[8] Bildik S, Dieter S, Fritzsch C, et al. Reconfigurable folded reflectarray antenna based upon liquid crystal technology. IEEE Trans Antennas Propagat. 2015;63(1):122–132. DOI:10.1109/TAP.2014.2367491
[9] Lavrentovich OD. Topological defects in dispersed liquid crystals, or words and worlds around liquid crystal drops. Liq Cryst. 1998;24(1):117–126. DOI:10.1080/026782998207640
[10] Seč D, Porenta T, Ravnik M, et al. Geometrical frustration of chiral ordering in cholesteric droplets. Soft Matter. 2012;8(48):11982–11988. DOI:10.1039/c2sm27048j
[11] Senyuk B, Liu Q, He S, et al. Topological colloids. Nature. 2013;493(7431):200–205. DOI:10.1038/nature11710
[12] Mundoor H, Senyuk B, Smalyukh I. Triclinic nematic colloidal crystals from competing elastic and electrostatic interactions. Science. 2016;352(6281):69–73. DOI:10.1126/science.aaf0801
[13] Castles F, Day F, Morris S, et al. Blue-phase templated fabrication of three-dimensional nanostructures for photonic applications. Nat Mater. 2012;11(7):599–603. DOI:10.1038/nmat3330
[14] Tkalec U, Ravnik M, Čopar S, et al. Reconfigurable knots and links in chiral nematic colloids. Science. 2011;333(6038):62–65. DOI:10.1126/science.1205705
[15] Araki T, Buscaglia M, Bellini T, et al. Memory and topological frustration in nematic liquid crystals confined in porous materials. Nat Mater. 2011;10(4):303–309. DOI:10.1038/nmat2982
[16] Stratford K, Henrich O, Lintuvuori J, et al. Self-assembly of colloid-cholesteric composites provides a possible route to switchable optical materials. Nat Commun. 2014;5. DOI:10.1038/ncomms4954
[17] Muševič I. Liquid-crystal micro-photonics. Liq Cryst Rev. 2016;4(1):1–34. DOI:10.1080/21680396.2016.1157768
[18] Lee T, Mundoor H, Gann DG, et al. Imaging of director fields in liquid crystals using stimulated Raman scattering microscopy. Opt Express. 2013;21(10):12129–12134. DOI:10.1364/OE.21.012129
[19] Smalyukh I, Shiyanovskii S, Lavrentovich O. Three-dimensional imaging of orientational order by fluorescence confocal polarizing microscopy. Chem Phys Lett. 2001;336(1–2):88–96. DOI:10.1016/S0009-2614(00)01471-8
[20] Higgins D, Luther B. Watching molecules reorient in liquid crystal droplets with multiphoton-excited fluorescence microscopy. J Chem Phys. 2003;119(7):3935. DOI:10.1063/1.1591716
[21] Collings P, Patel J. Handbook of liquid crystal research. New York (NY): Oxford University Press; 1997.
[22] Ondris-Crawford R, Boyko E, Wagner B, et al. Microscope textures of nematic droplets in polymer dispersed liquid crystals. J Appl Phys. 1991;69(9):6380. DOI:10.1063/1.348840
[23] Ackerman P, van de Lagemaat J, Smalyukh I. Self-assembly and electrostriction of arrays and chains of hopfion particles in chiral liquid crystals. Nat Commun. 2015;6:6012. DOI:10.1038/ncomms7012
[24] Posnjak G, Čopar S, Muševič I. Points, skyrmions and torons in chiral nematic droplets. Sci Rep. 2016;6:26361. DOI:10.1038/srep26361
[25] Orlova T, Aßhoff S, Yamaguchi T, et al. Creation and manipulation of topological states in chiral nematic microspheres. Nat Commun. 2015;6:7603. DOI:10.1038/ncomms8603
[26] Zhou Y, Bukusoglu E, Martínez-González J, et al. Structural transitions in cholesteric liquid crystal droplets. ACS Nano. 2016;10(7):6484–6490. DOI:10.1021/acsnano.6b01088
[27] Yoshioka J, Ito F, Tabe Y. Stability of a double twisted structure in spherical cholesteric droplets. Soft Matter. 2016;12(8):2400–2407. DOI:10.1039/C5SM02838H
[28] Jeong J, Davidson Z, Collings P, et al. Chiral symmetry breaking and surface faceting in chromonic liquid crystal droplets with giant elastic anisotropy. Proc

Natl Acad Sci. 2014;111(5):1742–1747. DOI:10.1073/pnas.1315121111

[29] Seč D, Čopar S, Žumer S. Topological zoo of free-standing knots in confined chiral nematic fluids. Nat Commun. 2014;5:3057. DOI:10.1038/ncomms4057

[30] Kleman M, Lavrentovich O. Soft matter physics. New York (NY): Springer; 2003.

[31] Čopar S, Porenta T, Žumer S. Visualisation methods for complex nematic fields. Liq Cryst. 2013;40(12):1759–1768. DOI:10.1080/02678292.2013.853109

[32] Drzaic P. Liquid crystal dispersions. Singapore: World Scientific; 1995.

[33] Čančula M, Ravnik M, Žumer S. Generation of vector beams with liquid crystal disclination lines. Phys Rev E. 2014;90(2):022503. DOI:10.1103/PhysRevE.90.022503